EXTENDING THEORETICAL TREATMENT OF RF VOLTAGE MODULATION TO NON-ZERO SYNCHRONOUS PHASE ANGLES

M. H. Wang*, SRRC, Hsinchu, 300, Taiwan
S.Y. Lee†, Department of Physics, Indiana University, Bloomington, IN 47405, U.S.A.

Abstract

Recently, RF voltage modulation has been successfully applied to suppress coupled bunch instabilities at Taiwan Light Source (TLS) a high current electron storage rings. Theoretical treatment of these systems need to be extended to non-zero synchronous phase angle. We study the effects of non-zero synchronous phase angle on the strengths of parametric resonances both in perturbation method and non-perturbatively. Experimental data obtained by using the Streak Camera will be compared with theoretical analysis. Systematic analysis of beam characteristics under rf voltage modulation will be presented.

1 INTRODUCTION

In the past few years, experimental measurements employing rf phase and voltage modulations have been carried out in many accelerator laboratories [1, 2, 3]. These works study the beam transfer function, resonance island bifurcation structure, hysteretic phenomena, etc. However, systematic experimental measurements of beam properties are limited, and theoretical description of these phenomena has remained within the framework of zero synchronous phase angle $\phi_{\rm s} = 0$ [4, 5]. However, the synchronous phase angle is non-zero in electron storage rings because of synchrotron radiation energy loss. The effect of non-zero synchronous phase angle has not been studied.

This paper reports physics and beam characteristics of applying rf voltage modulation with non-zero synchronous phase at the Taiwan Light Source (TLS), and systematically studies the resonance island bifurcation with rf voltage modulations. Section II reports the longitudinal beam dynamics with rf voltage modulation at a non-zero synchronous phase. The bifurcation of resonance islands will be systematically analyzed around the second synchrotron sideband. Section III shows the results of simulation of particle tracking at different synchronous phase and the numerical solution of Eq. (6). Section IV reports measurements of parametric resonances using streak camera for single bunch. Effects of beam characteristics will be systematic studied. Data obtained from experimental measurements are compared with theoretical description. Conclusion is reported in Sec. V.

* mhwang@srrc.gov.tw
† Email:shylee@indiana.edu

2 LONGITUDINAL BEAM DYNAMICS WITH RF VOLTAGE MODULATION

The synchrotron equations of motion, in the presence of rf voltage modulation, are given by

$$\frac{d\phi}{d\theta} = \nu_{\rm s}\delta, \quad (1)$$

$$\frac{d\delta}{d\theta} = \frac{\eta}{|\eta|}\nu_{\rm s}\left[\{1+\epsilon\sin(\nu_{\rm m}\theta+\xi)\}\sin\phi - \frac{U}{eV_{\rm rf}}\right], \quad (2)$$

where ϕ and $\delta = -\frac{h|\eta|}{\nu_{\rm s}}\left(\frac{\Delta p}{p_0}\right)$ are conjugate phase space coordinates, the revolution angle $\theta = \omega_0 t$ serves as the independent variable, h is the harmonic number, η is the phase slip factor, $\nu_{\rm s} = \sqrt{h|\eta|eV_{\rm rf}/(2\pi\beta^2 E_0)}$ is the synchrotron tune at zero synchronous phase angle, p_0 and E_0 are the momentum and energy of a synchronous particle, $\Delta p = p - p_0$ is the momentum deviation, $V_{\rm rf}$ is the rf voltage, ϵ is the rf voltage modulation amplitude, $\nu_{\rm m} = f_{\rm m}/f_0$ is the modulation tune, $f_{\rm m}$ is the modulation frequency, $f_0 = \omega_0/2\pi$ is the revolution frequency of a synchronous particle. We expand the radiation energy-loss U per-revolution in Taylor series of $\Delta E = E - E_0$: $U \approx U_0 + W\Delta E + \cdots$, where $U_0 = C_\gamma \frac{E^4}{\rho}$, $C_\gamma = 8.85\times10^{-5}$ m/(GeV)^3, and $W = dU/dE|_{E=E_0}$. The synchronous phase angle $\phi_{\rm s}$ is determined by the energy loss per revolution, i.e.

$$eV_{\rm rf}\sin\phi_{\rm s} = U_0 + U_{\rm id} + k_{\rm loss}Ne^2, \quad (3)$$

where $U_{\rm id}$ is the energy loss in insertion devices such as wigglers and undulators, and $k_{\rm loss}$ is the loss factor [6]. Since acceleration cavities are discrete, the synchrotron motion can be better described by the mapping equation:

$$\phi_{n+1} = \phi_n + 2\pi\nu_{\rm s}\delta_n, \quad (4)$$

$$\delta_{n+1} = \delta_n + 2\pi\nu_{\rm s}[\{1+\epsilon\sin(\nu_{\rm m}\theta+\xi)\}\sin\phi_{n+1} - \sin\phi_{\rm s}] - \frac{4\pi\alpha}{\omega_0}\delta_n, \quad (5)$$

where the radiation damping factor is $\alpha = f_0 W/2$, and we assume $\eta > 0$ hereafter. At the operation condition of the SRRC storage ring at 1.5 GeV, the damping factor is much smaller than the synchrotron frequency, i.e. $\alpha \approx 200$ s^{-1} and $\omega_{\rm s} = 1.6\times10^5 s^{-1}$. When the quantum fluctuation due to synchrotron radiation, rf noises, and other intrabeam Coulomb scattering processes is included, the equilibrium distribution that obeys the Fokker-Planck equation is a function of the Hamiltonian [7]:

$$H = \frac{1}{2}\nu_{\rm s}\delta^2 + \nu_{\rm s}(\{1+\epsilon\sin(\nu_{\rm m}\theta+\xi)\}[\cos\phi - \cos\phi_{\rm s}] + (\phi-\phi_{\rm s})\sin\phi_{\rm s}). \quad (6)$$

The Hamiltonian can be separated into two parts:

$$H_0 = \frac{1}{2}\nu_{\rm s}\delta^2 + \nu_{\rm s}([\cos\phi - \cos\phi_{\rm s}] + (\phi - \phi_{\rm s})\sin\phi_{\rm s}), \quad (7)$$

$$H_1 = \nu_{\rm s}\epsilon\sin(\nu_{\rm m}\theta + \xi)[\cos\phi - \cos\phi_{\rm s}], \quad (8)$$

where H_0 is the unperturbed Hamiltonian and H_1 is a sinusoidal time dependent perturbation. The unperturbed Hamiltonian H_0 has a stable fixed point (SFP) at $\phi_{\rm sfp} = \phi_{\rm s}$ and $\delta_{\rm sfp} = 0$, and an unstable fixed point (UFP) at $\phi_{\rm ufp} = \pi - \phi_{\rm s}$ and $\delta_{\rm ufp} = 0$. The sinusoidal time dependent perturbation may produce parametric resonance islands near the center of the bucket and cause large perturbation to the Hamiltonian motion. We will analyze the synchrotron motion when $\nu_{\rm m} \approx 2\nu_{\rm s}$ in the next Section.

2.1 *Effective Hamiltonian near the second synchrotron sideband*

We expand the unperturbed Hamiltonian in Taylor series around the SFP, and transform the conjugate phase-space coordinates $(\varphi = \phi - \phi_{\rm s}, \delta)$ into action-angle coordinates $(\bar{J}, \bar{\psi})$ with

$$\delta = \sqrt{2\bar{J}}|\cos\phi_{\rm s}|^{1/4}\cos\bar{\psi}, \quad (9)$$

$$\varphi = \phi - \phi_{\rm s} = -\sqrt{2\bar{J}}|\cos\phi_{\rm s}|^{-1/4}\sin\bar{\psi}. \quad (10)$$

The unperturbed Hamiltonian becomes

$$H_0 \approx (\nu_{\rm s}|\cos\phi_{\rm s}|^{1/2})\bar{J} - \frac{\sqrt{2}\nu_{\rm s}J^{3/2}\sin\phi_{\rm s}}{12|\cos\phi_{\rm s}|^{3/4}}(3\sin\bar{\psi} - \sin 3\bar{\psi}) - \frac{1}{6}\nu_{\rm s}\bar{J}^2\sin^2\bar{\psi} + \cdots. \quad (11)$$

With the generating function:

$$F_2(\bar{\psi}, \tilde{J}) = \bar{\psi}\tilde{J} + G_3(\tilde{J})\cos 3\bar{\psi} + G_1(\tilde{J})\cos\bar{\psi}, \quad (12)$$

where

$$G_3(\tilde{J}) = \frac{\sqrt{2}}{36}\tilde{J}^{3/2}\sin\phi_{\rm s}|\cos\phi_{\rm s}|^{-5/4}, \quad (13)$$

$$G_1(\tilde{J}) = \frac{\sqrt{2}}{4}\tilde{J}^{3/2}\sin\phi_{\rm s}|\cos\phi_{\rm s}|^{-5/4}, \quad (14)$$

the new Hamiltonian *near* $\nu_{\rm m} \approx 2\nu_{\rm s}$ can be approximated by $\tilde{H} \approx \langle\tilde{H}_0\rangle + \tilde{H}_1$, where

$$\langle\tilde{H}_0\rangle = (\nu_s|\cos\phi_{\rm s}|^{1/2})\tilde{J} - \frac{\nu_{\rm s}}{16}\left(1 + \frac{5}{3}\tan^2\phi_{\rm s}^2\right)\tilde{J}^2, \quad (15)$$

$$\tilde{H}_1 = \frac{1}{4}\epsilon\tilde{J}\nu_{\rm s}|\cos\phi_{\rm s}|^{1/2}\left(1 + \frac{1}{3}\tan^2\phi_{\rm s}\right)\sin(2\tilde{\psi} - \nu_{\rm m}\theta - \xi), \quad (16)$$

where $(\tilde{J}, \tilde{\psi})$ are conjugate variables and $\langle\tilde{H}_0\rangle$ is the average of $\tilde{H}_0$ over $\tilde{\psi}$.

2.2 *Resonance rotating frame and parametric resonances*

Transform the Hamiltonian into resonance rotating frame with the generating function

$$F_2(\tilde{\psi}, J) = \left(\tilde{\psi} - \frac{\nu_{\rm m}}{2}\theta - \frac{1}{2}\xi - \frac{\pi}{4}\right)J, \quad (17)$$

the new Hamiltonian becomes

$$\bar{H} = \Delta J - \frac{1}{2}\alpha J^2 + GJ\cos(2\psi), \quad (18)$$

where (J, ψ) are conjugate phase-space coordinates, and the resonance proximity parameter Δ, nonlinear detuning parameter α, and the resonance strength G are given by

$$\Delta = (\nu_s|\cos\phi_{\rm s}|^{1/2} - \frac{\nu_{\rm m}}{2}), \quad (19)$$

$$\alpha = \frac{1}{8}\left(1 + \frac{5}{3}\tan^2\phi_{\rm s}\right), \quad (20)$$

$$G = \frac{1}{4}\epsilon\nu_{\rm s}|\cos\phi_{\rm s}|^{1/2}\left(1 + \frac{1}{3}\tan^2\phi_{\rm s}\right). \quad (21)$$

The stable fixed points (SFP) of the Hamiltonian (18) are

$$J_{\rm sfp} = \frac{1}{\nu_{\rm s}(3 + 5\tan^2\phi_{\rm s})}(24\nu_{\rm s}|\cos\phi_{\rm s}|^{1/2} - 12\nu_{\rm m} + 2\epsilon\nu_{\rm s}|\cos\phi_{\rm s}|^{1/2}(3 + \tan^2\phi_{\rm s})), \quad (22)$$

if $\nu_{\rm m} < \nu_{\rm bif+}$, and $J_{\rm sfp} = 0$, if $\nu_{\rm m} > \nu_{\rm bif+}$ and $\nu_{\rm m} \leq \nu_{\rm bif-}$, where

$$\nu_{\rm bif+} = 2\nu_{\rm s}|\cos\phi_{\rm s}|^{1/2} + \frac{1}{2}\nu_{\rm s}\epsilon|\cos\phi_{\rm s}|^{1/2}(1 + \frac{1}{3}\tan^2\phi_{\rm s}), \quad (23)$$

$$\nu_{\rm bif-} = 2\nu_{\rm s}|\cos\phi_{\rm s}|^{1/2} - \frac{1}{2}\nu_{\rm s}\epsilon|\cos\phi_{\rm s}|^{1/2}(1 + \frac{1}{3}\tan^2\phi_{\rm s}). \quad (24)$$

The unstable fixed points (UFP) are given by

$$J_{\rm ufp} = \frac{1}{\nu_{\rm s}(3 + 5\tan^2\phi_{\rm s})}(24\nu_{\rm s}|\cos\phi_{\rm s}|^{1/2} - 12\nu_{\rm m} - 2\epsilon\nu_{\rm s}|\cos\phi_{\rm s}|^{1/2}(3 + \tan^2\phi_{\rm s})) \quad (25)$$

if $\nu_{\rm m} < \nu_{\rm bif-}$, and $J_{\rm ufp} = 0$ if $\nu_{\rm bif+} > \nu_{\rm m} > \nu_{\rm bif-}$. These resonances correspond to the nonlinear Mathieu instability.

3 PARTICLE TRACKING

A particle tracking program was written by using the mapping function in Eq. (4) and (5). The parameters of storage ring at SRRC were used for simulation. The TLS at SRRC is a 1.5 GeV third generation light source. The rf cavity was operating at 499.6540 MHz at the harmonic number $h = 200$. The revolution frequency was 2.4983 MHz. The total rf voltage was 800 kV with two rf cavities each cavity operated in 400 kV. The momentum compaction factor of the TBA lattice was $\alpha_{\rm c} \approx 6.33 \times 10^{-3}$. The damping rate was 200 s^{-1}. The synchronous phase angle of 169 degree was used for simulation. The initial particles were uniformly distributed 100 $\times$ 100 in a rectangular

box of dimension $\phi \in [-\pi, \pi], \delta \in [-0.015, 0.015]$. The modulation frequency put into simulation was from 50.5 kHz to 52.5 kHz with 0.1 kHz as a step. The simulation results of J_{sfp} versus modulation frequency was shown in Fig. 1.

4 RF VOLTAGE MODULATION EXPERIMENTS WITH A SINGLE BUNCH

The experiments of rf voltage modulation was carried out in single bunch mode with beam current about 2 mA. A sinusoidal wave from HP 33120A function generator was split into two and applied to the rf voltage feedback loops of the low level rf system.

In this single bunch rf voltage modulation, the modulation frequency around the second harmonics of the synchrotron frequency was increased step by step from below. The ratio of modulation amplitude in each cavity were set at 0.083. However, the effective modulation amplitude may differ from the set value due to relative phase between these two modulation terms. Our data analysis indicated that the effective modulation amplitude was about $\epsilon \approx 0.026$. The beam response of the sinusoidal rf voltage modulation was recorded by the streak camera [8].

Since the buckets are separated by $\tau_{\rm sep} = 2001.3609$ ps, the maximum phase amplitude of the stable fixed point is given by $\hat{\varphi} = 2\pi\hat{\Delta}t/\tau_{\rm sep}$, where $\hat{\Delta}t$ is the amplitude of the beamlet oscillation in ps. The action of the fixed point is then given by Eq. (10), i.e.

$$J_{\rm sfp} = \frac{1}{2}\,\hat{\varphi}^2 |\cos\phi_s|^{1/2}. \qquad (26)$$

The frequency response ($J_{\rm sfp}$) of rf voltage modulation of single bunch is shown in Fig. 1 for an effective modulation amplitude of $\epsilon = 0.026$. The frequency of sinusoidal rf voltage modulation was increased from below. As the modulation frequency reached a certain value below the second harmonic of the rf frequency, the beam would split into three beamlets [1]. The center beamlets vanished at modulation frequency of $f_{\rm bif-} = f_0\nu_{\rm bif-}$ of 51.0. As the modulation frequency is increased beyond $f_{\rm bif-}$, the beam was observed to split into two beamlets in each bucket as predicted by the Mathieu instability discussed in Sec. 2.2. When the modulation frequency was higher than 51.65, the Mathieu instability disappeared and the beam becomes a single bunch in the bucket.

It was also found the beam would split into two beamlets first when modulation frequency was swept from above reaching the bifurcation point $f_{\rm bif+}$ of Mathieu instability. As the frequency was tuned to below the 51.0. the amplitude of these two beamlets continued to increase until the outer islands became too small. This hysteretic phenomenon has been observed in many earlier experiments [1, 4].

5 CONCLUSION

We developed a theoretical description of rf voltage modulation on synchrotron motion with a non-zero synchronous phase angle. The resonance bifurcation of the rf bucket has been systematically studied. Near the second synchrotron sideband, the bifurcation is equivalent to the nonlinear Mathieu instability. We also found that the non-zero synchronous phase angle can also drive odd-order modes. The difference of the results of puertubative solution and the simulation results shown in Fig. 1 is due to the higher order detuning effects(see Eq. (15)). Our analysis can be easily applied to higher order parametric resonances.

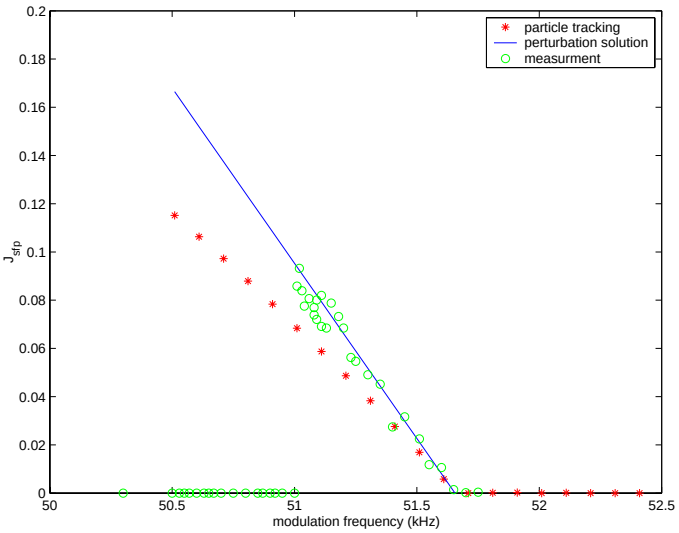

Figure 1: The action of the stable and unstable fixed points of single bunch beam under rf voltage modulation with synchrotron frequencies 25.66 kHz. The effective modulation amplitude was about $\epsilon \approx 0.026$ and the synchronous phase angle was about $\phi_{\rm s} = 169.0°$. The star data is result of particle tracking. The solid (SFP) and dashed (UFP) lines are obtained from perturbation theory shown in Eqs. (22) and (25). The circle data is from single bunch measurement.

6 REFERENCES

[1] M.H. Wang *et al.*, Ph.D. Thesis, Tsing-Hua University, Taiwan, 1998, unpublished; Proceedings of the Particle Accelerator Conference (PAC) 1997, p. 1487; Proceedings of PAC 1999, p. 2837 (1999).

[2] J. Byrd *et al.*, Phys. Rev. E**57**, 4706 (1998).

[3] J. Chen *et al*, Proceedings of PAC 1999, p. 2412 (1999).

[4] D. Li, et al., Phys. Rev. E**48**, R1638 (1993); D. Li, et al., Nucl. Instr. and Meth. **A364**, 205(1995).

[5] S.Y. Lee, *Accelerator Physics*, (World Scientific Co., 1999)

[6] A. Chao, in *Physics of Collective Beam Instabilities in High Energy Accelerators* (Wiley, New York, 1993).

[7] M. Bai *et al.*, Phys. Rev. E**55**, 3493 (1997).

[8] M.H. Wang *et al.*, Proceedings of the PAC 1995, p. 2971 (1995); M.H. Wang *et al.*, Proceedings of the European particle Accelerator Conference (EPAC) 1996, p. 1120 (1996);